Construction of recombinant Pdu metabolosome shells for small molecule production in *Corynebacterium glutamicum*

Isabel Huber[†], David J. Palmer[‡], Kira N. Ludwig[†], Ian R. Brown[‡], Martin J. Warren[‡] and Julia Frunzke[†*]

[†]Institute of Bio- and Geosciences, IBG-1: Biotechnology, Forschungszentrum Jülich, Jülich, Germany

[‡]School of Biosciences, University of Kent, Giles Lane, Canterbury, Kent CT2 7NJ, U.K.

*Address correspondence to j.frunzke@fz-juelich.de

Keywords: Bacterial microcompartments, propanediol utilization, metabolic engineering, protein encapsulation, *C. glutamicum*;

1 Abstract

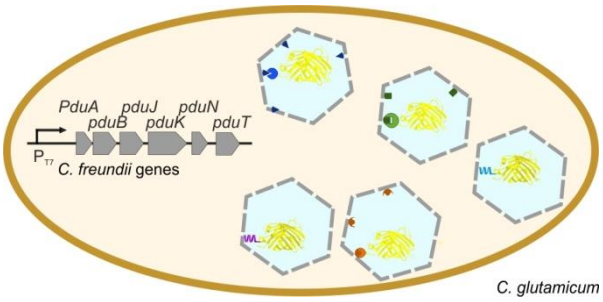

Bacterial microcompartments have significant potential in the area of industrial biotechnology for the production of small molecules, especially involving metabolic pathways with toxic or volatile intermediates. *Corynebacterium glutamicum* is an established industrial workhorse for the production of amino acids and has been investigated for the production of diamines, dicarboxylic acids, polymers and bio-based fuels. Herein, we describe components for the establishment of bacterial microcompartments as production chambers in *C. glutamicum.* Within this study, we optimized genetic clusters for the expression of the shell components of the *Citrobacter freundii* propanediol utilization (Pdu) bacterial compartment, thereby facilitating heterologous compartment production in *C. glutamicum*. Upon induction, transmission electron microscopy images of thin sections from these strains revealed microcompartment-like structures within the cytosol. Furthermore, we demonstrate that it is possible to target eYFP to the empty microcompartments through C-terminal fusions with synthetic scaffold interaction partners (PDZ, SH3 and GBD) as well as with a non-native C-terminal targeting peptide from AdhDH (*Klebsiella pneumonia*). Thus, we show that it is possible to target proteins to compartments where N-terminal targeting is not possible. The overproduction of PduA alone leads to the construction of filamentous structures within the cytosol and eYFP molecules are localized to these structures when they are N-terminally fused to the P18 and D18 encapsulation peptides from PduP and PduD, respectively. In future, these nanotube-like structures might be used as scaffolds for directed cellular organization and pathway enhancement.

2 Introduction

The integration of synthetic pathways into different bacterial chassis organisms is often associated with the appearance of toxic intermediates that interfere with the metabolism of the host. Eukaryotic cells have evolved a wide range of different organelles for distinct functions to encapsulate specific metabolic pathways within the cell, thereby avoiding competition with other cytoplasmic processes. Remarkably, genomic analyses suggest that about 20% of bacterial species contain proteinaceous microcompartments (BMCs) as distinct reaction chambers (*1*).

BMCs fall into one of two distinct classes depending on whether they encode for anabolic or catabolic processes, which are known as carboxysomes and metabolosomes, respectively (*2*). Carboxysomes are associated with the anabolic process of carbon dioxide fixation and help to generate elevated CO_2 levels within the BMC by enclosing carbonic anhydrase and RuBisCO, thereby enhancing carbon fixation into 3-phosphoglyceraldehyde (*3*). Metabolosomes are associated with catabolic reactions and genetic evidence suggests there are at least 10 distinct BMC-encapsulated metabolic processes. Of these, only a few have been experimentally characterized to any extent, including those for propanediol utilization (Pdu), ethanolamine utilization (Eut), fucose/rhamnose utilization, and choline utilization (*2, 4*).

Of these, the best studied is the Pdu metabolosome system from *Salmonella enterica* and *Citrobacter freundii.* The catabolism of 1,2-propanediol involves its disproportionation into propionic acid and propanol via propionaldehyde. Encasing the degradative pathway for 1,2-propanediol into a BMC allows the reactive and volatile propionaldehyde intermediate to be sequestered, thereby preventing cellular toxicity and carbon loss (*5*). The *C. freundii* Pdu operon consists of 23 genes, which code not only for the metabolic pathway enzymes for 1,2-propanediol degradation but also for the reactivation and recycling of cofactors. The Pdu operon also contains seven genes that encode for eight shell proteins (PduA,B,B',J,K,N,U,T) (*6*). The Pdu shell proteins fall into one of three categories, depending on whether they form hexamers (BMC-H), pentamers (BMC-P) or trimers (BMC-T). It is suggested that the hexameric and trimeric shell proteins assemble into extended flat sheets, which form the facets

of assembled compartments. BMC-H proteins are proposed to have selectively permeable central pores with a diameter of ~6 Å that allow the passage of substrate and product across the shell, but prevent the efflux of toxic or volatile intermediates (*7*). BMC-T proteins have allosterically regulated pores, whereby the open form provides a triangular central pore with a diameter of 8-11 Å. These larger pores provide the opportunity to allow the entry of enzymatic cofactors such as NAD and CoA (*8, 9*). The group of pentameric BMC-P proteins is thought to form the vertices of the structure and thereby facilitate the closure of the overall structure (*9*). Several studies highlight the importance of a specific protein ratio of the different organelle shell proteins for a proper high order assembly (*10, 11*).

In recent years, researchers also realized the potential of BMCs for the establishment of synthetic nanobioreactors within a microbial production host. Several studies benchmarked the heterologous assembly of empty compartments in *E. coli* through the expression of the shell genes of the Pdu compartment from *C. freundii* (*12, 13*), the Eut compartment from *Salmonella enterica* (*14, 15*) and a microcompartment of unknown function from *Haliangium ochraceum (16)*.

The transferability of the compartment shell assembly across different proteobacterial classes emphasizes the modular nature of BMCs and offers an opportunity for engineered small molecule production. To improve microbial productivity in strains with subcellular compartments, the incorporation of heterologous pathway enzymes into the compartment lumen is an important requirement. In the native hosts, encapsulation peptides localize specific pathway enzymes to the BMC lumen (*17*). Encapsulation peptides typically range from 15-20 amino acids and form an α-helix of amphipathic nature that is linked to the rest of the protein by a poorly conserved linker sequence (*18, 19*). They are found normally at the N- and occasionally at the C-terminus of the protein and are specific for microcompartment-associated enzymes. It is proposed that the characteristic pattern of hydrophilic and hydrophobic residues of the encapsulation peptide plays a major role in its interaction with the shell proteins (*19, 20*). For the Pdu system, several reports have shown that the first eighteen residues of PduP (P18) and PduD (D18) are able to localize GFP and several other cargo enzymes into the

compartment lumen (*12, 17, 21*). Nevertheless, a current challenge to any application is that N-terminal encapsulation peptides (P18 and D18) can negatively affect recombinant enzymes with regard to specific activity, solubility and the formation of inclusion bodies (*21*). Efficient synthetic design demands an enlargement of the targeting peptide repertoire in order to provide optimized solutions for the particular proteins.

In the first publication on the redesign of a BMC to house a non-natural pathway researchers were able to produce elevated amounts of ethanol in *E. coli* by the introduction of an alcohol dehydrogenase (AdhB) and a pyruvate decarboxylase (Pdc) from *Zymomonas mobilis* targeted to an empty *C. freundii* Pdu compartment (*12*). BMCs have also been engineered to enhance biomineralisation processes through polyphosphate accumulation (*22*) and toxic protein accumulation through the production of lysis protein E (*23*). However, it is clear that the recombinant production of BMCs is difficult which explains why there have been comparatively few applied processes reported so far.

Corynebacterium glutamicum represents an important host for bioproduction processes. Per year, more than five million tons of amino acids (mainly L-glutamate and L-lysine) are produced with this host (*24*). Furthermore, *C. glutamicum* has been successfully engineered for the production of further value-added products, including diamines, dicarboxylic acids, polymer precursors and bio-based fuels such as ethanol (*25*). The development of synthetic BMCs in this industrial platform strain could expand the repertoire of *C. glutamicum* production strains, especially to products whose synthesis involves toxic or volatile intermediates. To the best of our knowledge, all studies on the establishment of recombinant engineered metabolosomes to date have been performed in the gram-negative *E. coli* with compartments of proteobacterial origin. In this study, we have chosen the prophage-free *C. glutamicum* MB001(DE3) strain to establish synthetic Pdu compartments derived from the *C. freundii* Pdu system in this Gram-positive model organism. Furthermore, we provide alternative targeting strategies that expand the synthetic repertoire for targeting proteins into the compartment lumen.

3 Results and Discussion

Different Pdu operon designs lead to diverse fluorescence patterns in *C. glutamicum*

In this study, we aimed to produce recombinant Pdu BMCs in the biotechnologically important organism *C. glutamicum*. Initially, we introduced the *C. freundii* Pdu operon into *C. glutamicum* on a plasmid to test the transferability of this system to a Gram-positive organism. To this purpose, we focused on three basic designs: First, the central 21 gene-component of the operon, *pduA-X* (*11*), was cloned into a pAN6 vector under control of the inducible P_{tac} promoter. Second, the empty shell operon *pduABJKNUT* (*13*) was cloned under the control of an IPTG inducible P_{T7} promoter in the plasmid pMKEx1. The genes within the synthetic operon contain 40 bp upstream regions including a ribosome binding site, which are located in front of *pduAB*, p*duJ*, *pduK*, *pduN*, *pduU* and *pduT* (*13*). As a third variant, the synthetic operon was placed under control of the native 3' untranslated regions (3'UTR) of the genes that encode the shell proteins (*pduABJKNTU*$_{native}$, Fig. 1A).

As revealed in previous studies, proteins of interest can be targeted into the BMC lumen by fusing them to the first 18 amino acids of the enzymes PduP or PduD (further named P18 and D18, respectively) (*12, 17, 20, 21*). Using this approach, we visualized the structures resulting from the expression of the aforementioned operons in *C. glutamicum* MB001(DE3) by coproduction with P18eYFP (Fig. 1B) using wide field fluorescence microscopy. For the 21 gene construct containing *pduA-X*, filamentous structures as well as adjacent round structures were observed after 4 hrs of induction. As a control, no interaction was observed when untagged eYFP was coproduced with PduA-X. Here, the eYFP signal was evenly distributed within the cytosol. The coproduction of a construct containing only genes for the shell proteins with their native upstream regions (PduABJKNTU$_{native}$) and P18eYFP resulted in the formation of similar structures as observed with PduA-X. These findings, however, suggest some kind of assembly problem with the Pdu BMCs within the cell. Previous studies have also reported the formation of aberrant structures within cells, including the appearance of laminar features with

158 the overexpression or deletion of single or multiple shell protein genes (*13, 26*). In an *E. coli*
159 strain containing *pduA-X*, further overexpression of individual shell proteins (PduA,-B,-B',-J,-
160 K,-U,-T), apart from PduN, was shown to have a negative influence on compartment assembly
161 (*11*). Based on these observations, it can be assumed that imbalances in protein stoichiometry
162 hinder the correct assembly of Pdu BMCs.
163 The expression of the synthetic shell operon *pduABJKNUT, together* with P18eYFP, produced
164 distinct foci within the cytosol, consistent with the formation of BMC structures. However,
165 further inspection of strain MB001(DE3) *pduABJKNUT* by transmission electron microscopy,
166 revealed the presence of large and unstructured aggregates with no defined borders in the
167 majority of the cells (Fig. 2B). 'BMC-like' structures were observed in around 4% of cells, but
168 these are likely to be artefacts from embedding or volutin granules (*27*) as these structures
169 were also observed within 4% of the control strain, MB001(DE3) (Fig. S1 and Table S2).

170 **Optimization of protein stoichiometry for compartment assembly**

171 To prevent the production of aggregates and misshaped BMC protein assemblies we
172 attempted to optimize protein stoichiometry in order to facilitate proper assembly in
173 *C. glutamicum*. Based on the analysis of the molar ratios of the Pdu shell proteins purified from
174 *S. enterica* (*28*), the shell proteins were classified into three groups; high abundancy
175 (PduA,B,B',J; ~16-28 % each), low abundancy (PduK,U,T; ~3 % each) and minor abundancy
176 (PduN, not detectable) (*28*). Changes in protein stoichiometry were achieved by modification
177 of the start codons of single or combinations of shell genes from ATG (100%) to GTG (~40%
178 translation efficiency in relation to the usage of ATG) (*29*) for *pduK*, *pduU* and *pduT*, or TTG
179 (~1% in relation to ATG) (*29*) for *pduN.* This was combined with the deletion of *pduU* and/or
180 *pduT*. Hereafter, small letters within the operon notation are used to represent these changes
181 of the start codons. Eight operon versions based on *pduABJKNUT* were designed and are
182 presented in Fig. 2.
183 After transfer into *C. glutamicum,* the effect of these 8 operons were then individually analyzed
184 for BMC formation (Fig. 2). Thin sections of MB001(DE3) *pduABJKNUT* (Fig. 2B), *pduABJKnut*
185 (Fig. 2C), and *pduABJKnt* (Fig. 2D), displayed similar phenotypes in that they were observed

to contain aggregated protein rather than BMC-like structures. Even though these structures are apparently not inclusion bodies, which normally appear as round structures at the cell poles, these samples lack the defined edges normally associated with fully assembled BMCs. In all strains containing plasmids where PduK was downregulated thin sections of cells revealed compartment-like structures with defined borders (Fig. 2E-J). Thus, it can be concluded that a reduction in the levels of PduK, was a key step to successful compartment assembly in *C. glutamicum*. In *E. coli,* PduK was shown to be essential for compartment formation (*13*) but the overexpression of *pduK* led to large aggregates with delimiting boundaries (*11*). The 'fluffy' phenotype of the shell proteins we observed in this study appears to be exclusive to *C. glutamicum* and might be related to the impact of using a non-native host system for BMC production.

In contrast, modulation of PduN abundancy had no visible effect on compartment formation. This can be seen by comparing the thin sections of strains MB001(DE3) *pduABJkn* (Fig. 2I) with MB001(DE3) *pduABJkN* (Fig. 2J) as well as MB001(DE3) *pduABJknt* (Fig. 2G) with MB001(DE3) *pduABJkNt* (Fig. 2H). Our data are in agreement with previous *E. coli* studies which also showed that levels of PduN had no significant impact on BMC formation (*11*).

Interestingly, the cells of all strains containing *pduU* produced a yellow pigment to give a yellow phenotype, even when the heterologous gene was not induced (Fig. S2). The yellow pigment is presumably some kind of stress response. These strains also had reduced growth rates when compared to strains lacking *pduU* and induced with 50 µM IPTG (Fig. S2). As a result, we looked at the influence of *pduU* on compartment assembly by comparing the strains expressing *pduABJkNu* (Fig. 2F), *pduABJkN* (Fig. 2J), *pduABJkNut* (Fig. 2E) and *pduABJkNt* (Fig. 2H). Analysis of thin sections of cells revealed no obvious differences that correlated with the presence or absence of PduU. In contrast, thin sections of strains containing *pduT* within the operon revealed more distinct borders that helped define the individual compartments (compare *pduABJkNut* (Fig. 2E) with *pduABJkNu* (Fig. 2F), *pduABJknt* (Fig. 2G) with *PduABJkn* (Fig. 2I) and *pduABJkNt* (Fig. 2H) with *pduABJkN* (Fig. 2J)).

To quantify the formation of BMCs in the different strains, cells were accounted to contain 'BMC'-like structures, if they contained a minimum of one closed BMC. Cells in which either no or only misshaped structures were observed, were counted to contain no BMCs (Table S2). Of the two strains lacking both PduU and PduT, 26% and 29% of the cells were found to include BMC-like structures, whereas in MB001(DE3) *pduABJkNt* and MB001(DE3) *pduABJknt,* both of which contain *pduT*, and in MB001(DE3) *pduABJkNut* which contains both *pduU* and *pduT,* the number of cells containing visible BMC-like structures was higher (38%, 46% and 53% respectively). Thus, PduU and PduT were found to be dispensable for successful compartment formation (*13, 30*) although a reduction of PduT levels may help form clearer borders.

Based on these data, we consider that the structures observed in ~50% of the cells from MB001(DE3) *pduABJkNut* and *pduABJknt* represent arrangements of compartment-like structures with delimiting boundaries (Fig. 2E, Fig. 2G and Table S2), whilst some structures produced within these strains seem to be poorly formed, not fully closed and vary in size. The observed BMCs are arranged together in the mid part of the cell, rather than being distributed across the cytoplasm, which is similar to the clustering of heterologously produced BMCs in *E. coli* (*12, 13, 21*). This may be a consequence of the high expression levels in heterologous systems, whereas BMC production in native hosts is more tightly regulated (*31*). For Pdu BMCs, PduV was shown to localize to the outside of BMCs and to be responsible for their movement within the cytoplasm (*13*). Therefore, the implementation of this protein into the heterologous system might be considered for proper BMC distribution.

To confirm BMC shell assembly further, attempts were made to isolate compartments from MB001(DE3) *PduABJknt* using a previously published procedure (*12*). Major difficulties were encountered in trying to lyse *C. glutamicum* cells prior to the subsequent steps of the purification protocol. Effective cell lysis of *C. glutamicum* requires the application of mechanical disruption methods such as sonication or French Press. However, these approaches are known to compromise the integrity of BMCs. Attempts to obtain BMCs from *E. coli* using sonication to lyse the cells have only yielded very poor quality BMCs. Nonetheless, purification of BMCs from *C. glutamicum* was attempted using sonication as a lysis method. Some partially

purified BMC proteins were obtained by following the BMC purification protocol. However, the protein yield was very low and only 3 shell proteins could be detected by SDS gel electrophoresis (Fig. S3). Overall, this purification approach was hampered by the thick *C. glutamicum* cell wall and did not significantly contribute to the verification of functionally assembled compartment structures. Furthermore, the presence of lipid impeded the identification of BMCs by TEM.

Chromosomal integration of the *pduABJknt* shell operon

In order to generate a more stable expression system, the optimized *pdu* shell operon, *pduABJknt,* under control of the P_{T7} promoter, was integrated into an intergenic region on the chromosome of *C. glutamicum* MB001(DE3), between the genes cg1121 and cg1122. The growth performance of the resulting strain was tested with different IPTG inducer concentrations and compared to the MB001(DE3) strain (Fig. 3A). For the control strain MB001(DE3), the growth rates in the absence and presence of 150 µM IPTG were very similar at 0.548 ± 0.008 h^{-1} and 0.540 ± 0.003 h^{-1} respectively. With increasing IPTG levels a moderate influence on the growth rate of MB001(DE3)::P_{T7}*pduABJknt* was observed (0.558 ± 0.011 h^{-1} without IPTG induction, 0.522 ± 0.005 h^{-1} with 20 µM IPTG, 0.452 ± 0.009 h^{-1} with 50 µM IPTG and 0.428 ± 0.009 h^{-1} with 150 µM IPTG). Compartment production was investigated by fluorescence microscopy after induction of the Pdu operon with 50 µM IPTG and the coproduction of different eYFP versions. In the control strain MB001(DE3) *pduABJknt eyfp*, eYFP fluorescence was evenly distributed throughout the cytoplasm (Fig. 3B). We were able to observe that P18eYFP and D18eYFP both localized to foci within the cell when coproduced with PduABJknt (Fig. 3B). The formation of such foci is consistent with the colocalisation of eYFP to BMCs. Additionally, an SsrA-degradation tag variant, AAEKSQRDYAASV (ASV) (*32*), was fused to the C-terminus of D18eYFP and P18eYFP to generate D18eYFP$_{ASV}$ and P18eYFP$_{ASV}$. The addition of this tag makes the proteins susceptible to tail-specific proteases in the cytoplasm (*33*), whilst encapsulation of such proteins would protect them from degradation. When D18eYFP$_{ASV}$ was coproduced with the shell proteins, eYFP was protected from degradation as fluorescence foci were observed within the cell (Fig. 3B). This is consistent

with D18eYFP$_{ASV}$ being encapsulated within a BMC. Similar results were obtained with the maximal expression (250 µM IPTG) of the operon (Fig. S4). TEM analysis of MB001(DE3)::P$_{T7}$*pduABJknt* revealed BMC-like structures in 19% of the cells examined (Fig. 3C). However, the boundaries of the BMC-like structures were not as distinct as seen with the plasmid-based BMC production strain MB001(DE3) *pduABJknt* (Fig. 2G).

C-terminal targeting to BMCs is possible with native and non-native encapsulation peptides

It would be of advantage to have the option to choose between N- and C-terminal tags for the encapsulation of heterologous pathways into BMCs. This is important as the addition of targeting peptides often influences enzymatic activity ((*21*) and Table 1).

Native targeting peptides have been described as amphipathic α-helices at the N- or C-terminus of enzymes. The proposed common mechanism is the interaction of the peptides with C-terminal α-helices of certain shell proteins or the epitopes of hexamer-hexamer interfaces (*18, 19*). Therefore, we wanted to investigate if the interaction of the P18 peptide with the shell proteins is still possible when it is moved to the C-terminus of the fluorescent protein. Additionally, two putative encapsulation peptides natively present at the C-terminus of the aldehyde dehydrogenases (AdhDH) of compartments of unknown function from *Klebsiella pneumonia* (C17$_{K.p.}$) and *Proteus mirabilis* (C17$_{P.m.}$) (*19*) were tested. The composition of hydrophilic and aliphatic amino acids is very similar between the selected encapsulation peptides from AdhDH and the P18/D18 peptides (Table S3). Fluorescence microscopy indicated the localization of eYFP to compartments when it is fused with a C-terminal P18 or C17$_{K.p.}$ peptide, although the localization is more distinct with eYFP-P18 (Fig. 4). With the C-terminal AdhDH sequence from *P. mirabilis*, the localization of eYFP was dispersed across the cytoplasm rather than being localized to the compartments. With these fluorescence microscopy studies, we cannot state to which extent eYFP-P18 and eYFP-C17$_{K.p.}$ are incorporated in comparison to P18eYFP. Nevertheless, these results suggest that the P18 and C17$_{K.p.}$ peptides may be used as C-terminal fusion for the targeting of cargo protein into the PduABJknt lumen.

Implementation of protein scaffolds for BMC targeting

Non-catalytic synthetic scaffolding proteins can provide engineered interactions between proteins. For example, combinations of interaction ligands and domains (namely PDZ, GBD and SH3 interaction partners) were utilized by Dueber *et al.* to target pathway enzymes to synthetic complexes (*34*). To enlarge the toolbox for synthetic BMC targeting peptides, we tested the suitability of these scaffolds to target a fluorescence reporter (tagged with the interaction domain) into the BMC lumen *via* PduA (tagged with the cognate interaction peptide ligand). For this purpose, the operon *pduABJknt* was adapted as follows: one of the three ligands (PDZlig, 7 aa, K_d = 8 µM (*34*); GBDlig, 32 aa, K_d = 1 µM (*34*); SH3lig, 11 aa, K_d = 0.1 µM (*34*)) was C-terminally fused to PduA and an additional ribosome binding site was inserted between *pduA* and *pduB*, because the two genes overlap in the original operon structure. To verify that the addition of the ligand does not interfere with the compartment assembly, TEM analysis was performed with MB001(DE3) *pduA*$_{PDZlig}$*BJknt* (Fig. 5A), MB001(DE3) *pduA*$_{GBDlig}$*BJknt* (Fig. 5B) and MB001(DE3) *pduA*$_{SH3lig}$*BJknt* (Fig. 5C). The images provide evidence that the strains are able to form compartment-like structures with the additional ligands fused to PduA and were of similar shape as those produced in MB001(DE3) *pduABJknt*. Depending on the nature of the ligand at the C-terminus of PduA, BMC-like structures are observed in 58% (for PDZ), 34% (for GBD) and 23% (for SH3) of the cells suggesting a measurable effect of the addition of synthetic scaffolds. However, it has to be noted that misshaped structures and protein aggregates appeared in a considerable fraction of cells of all imaged samples (Fig. S5).

To test for intracellular colocalisation, plasmids for the production of the BMC shell operons were cotransferred with plasmids encoding the cognate eYFP$_{PDZdom}$, eYFP$_{GBDdom}$ and eYFP$_{SH3dom}$ interaction partners (PDZdom, 95 aa; GBDdom, 79 aa; SH3dom, 58 aa). For all three strains, the respective eYFP$_{dom}$ signal localized within the mid part of the cells suggesting that they had been entrapped within the compartments (Fig. 5D). As a control, *D18eyfp* and *P18cfp* were separately cotransferred with *pduA*$_{lig}$*BJknt* into MB001(DE3) and upon BMC and eYFP production, D18eYFP and P18CFP were observed to localize to the compartments with

fluorescence patterns similar to those seen with $eYFP_{dom}$. It appears that the addition of the C-terminal ligand does not interfere with interactions of PduA during BMC assembly or the functionality of native D18 or P18 peptides. Thus, in principle, both the C- and N-terminal versions can be combined to target different proteins into the lumen of $PduA_{PDZ}$BJknt, as this strain showed the highest number of cells with BMCs. Furthermore, preliminary experiments on $AdhB_{dom}$ enzyme activities emphasize a positive influence of the C-terminal targeting on enzyme activities in comparison to the N-terminal targeting (Fig. S6).

PduA and PduJ form filaments in *C. glutamicum*

It has previously been shown that the recombinant overexpression of *C. freundii pduA* in *E. coli* results in the appearance of nanotube-like structures within the cytoplasm (*13, 26*). The use of PduA filaments as protein scaffolds for the localization of key metabolic pathway enzymes was therefore considered for *C. glutamicum.* Targeting of specific proteins of interest to PduA scaffolds could enhance metabolic pathway flux by substrate channeling and microdomain organization (*35-38*).

In our study, PduA was overproduced in *C. glutamicum* MB001(DE3) *pduA* after 4 hrs of induction with 50 µM IPTG. TEM analysis of thin sections revealed that PduA did form large bundles of regular filaments within the cell with a diameter of ~ 17-20 nm for single filaments (Fig. 6A). Since PduJ shares 80% sequence similarity to PduA it was investigated whether PduJ is also able to form filaments in *C. glutamicum*. TEM of thin sections of cell overproducing PduJ shows regular and linear filamentous structures (20 ± 5 nm in diameter) as well as large linear structures which may be a mixture of rolled protein sheets and filaments with a diameter of 4 ± 1.3 nm (Fig. 6B). The finding that PduJ not only forms filaments but also angular structures is consistent with the opinion that PduJ is present at the edges to join the facets of the compartments allowing complete closure of the compartment (*30*).

N-terminal targeting peptides recruit eYFP to PduA scaffolds

PduA and PduJ both include a C-terminal amphipathic motif, which is thought to interact with the P18 and D18 peptides (*20*). To investigate the interaction of both targeting peptides with

the PduA and PduJ structures in *C. glutamicum*, the genes were coexpressed with either *P18eyfp* or *D18eyfp*. Fluorescence microscopy analysis of the resulting strains proved the recruitment of the reporter proteins D18eYFP and P18eYFP to PduA tubes (Fig. 6C). However, no localization of these reporter proteins to PduJ filaments was observed. The visible dots may represent eYFP molecules targeted to the angular structures observed *via* TEM (Fig. 6B), but these structures might also represent inclusion bodies formed by aggregated P18eYFP and D18eYFP proteins (Fig. 6D) since targeting peptides tend to aggregate together (*21*). The fluorescence microscopy approach does not conclusively indicate if PduJ is a target of the encapsulation peptides, P18 or D18. With regard to an application of the shell proteins as a scaffold, PduA seems to be the more promising candidate. To have a stable PduA production strain, the *pduA* gene was genomically integrated into the same genomic locus as described previously for *pduABJknt*. Growth curves show a significant influence of the PduA production on cellular growth when compared to the expression of the *pduABJknt* operon (Fig. 3A). It is likely that the filamentous structures have a significant impact on cell division by interfering with septation.

C-terminal targeting to PduA is possible by using PDZ and GBD interactions

To test if C-terminal targeting to PduA filaments is possible, PduA was fused with one of the three protein ligands (GBD, SH3 or PDZ) and coproduced with the cognate interaction domain attached to eYFP in *C. glutamicum* strain MB001(DE3). Coproduction of $PduA_{GBDlig}$ with $eYFP_{GBDdom}$ and $PduA_{PDZlig}$ together with $eYFP_{PDZdom}$ in MB001(DE3) resulted in successful targeting to the filaments, as visualized by fluorescence microscopy (Fig. 7). However, the coproduction of $PduA_{SH3lig}$ and $eYFP_{SH3dom}$ resulted in even distribution of fluorescence across the cytosol. To determine whether the SH3 ligand impairs filament assembly, $PduA_{SH3lig}$ was also coproduced with D18eYFP. Again no localization of fluorescence signal to filaments was observed, thus confirming that the addition of the SH3 ligand interferes with the assembly of the filamentous structures. As the fluorescence signal from D18eYFP coproduced with either $PduA_{PDZlig}$ or $PduA_{GBDlig}$ localizes to filaments, we assume that they are not restricted in their ability to assemble. Therefore $PduA_{PDZlig}$ and $PduA_{GBDlig}$ provide the option of targeting proteins

to PduA scaffolds with a C-terminal tag, via proteins fused to a PDZ/GBD domain, or N-terminally with a native P18 or D18 peptide tag.

Impact of PduABJknt BMCs on ethanol production in *C. glutamicum*

To evaluate the potential of BMCs in *C. glutamicum* for the production of small molecules, the encapsulation strategy with D18 and P18 targeting peptides and BMC production with MB001(DE3)::P_{T7}*PduABJknt* was applied in a proof-of-principle approach for ethanol production. This involves the localization of a *Z. mobilis* pyruvate decarboxylase (Pdc) and an alcohol dehydrogenase (AdhB) to the compartment. In order to localize the Pdc and AdhB to BMCs, both genes were fused with either the D18 or P18 EPs with different linker sequences and the respective genes placed under the control of a constitutive P_{tuf} promoter to achieve moderate expression.

We measured the influence of encapsulation peptides on enzyme activity. The specific activity of AdhB, D18-GSGS-AdhB D18-10aa-AdhB and D60-AdhB were determined in crude cell extracts of the respective MB001(DE3) strains. The highest specific activity was observed for the untagged AdhB version (0.376 ± 0.045 U mg^{-1} cell extract), the activities were almost depleted for all EP-tagged AdhB versions containing different linker sequences (0.021-0.067 U mg^{-1} cell extract) (Table 1). In contrast, the activity of pyruvate decarboxylases P18-NdeI-Pdc and P18-GSGS-Pdc in cell extracts of MB001(DE3) were not significantly influenced by the addition of the targeting peptide in comparison to the untagged Pdc version (Table 1). These data revealed significant differences on enzyme activity of the targeting peptides and, thus, highlight the importance of utilizing an encapsulation peptide toolbox for synthetic targeting approaches. For optimal enzymatic activity and BMC design, a variety of encapsulation peptides need to be tested on the particular protein of interest.

We transformed the BMC production strain MB001(DE3)::P_{T7}*pduABJknt* and the control MB001(DE3) strain with the plasmids P_{tuf}*adhB_pdc,* P_{tuf}*D18-GSGS-adhB/P18pdc* and P_{tuf}*D18-10aa-adhB/P18pdc*. The strains were cultivated in 50 mL CXII + 2% (w/v) glucose in 100 mL shaking flasks at 30°C and 140 rpm for 60 h. Because under aerobic conditions no ethanol was produced (data not shown), an increased filling volume to 50% of the maximum flask

capacity was applied to achieve a reduction of O_2 supply within the cultivation medium. The highest ethanol titers were measured after 48 hrs of cultivation (Fig. 8). MB001(DE3)::P_{T7}*pduABJknt* P_{tuf}*D18-10aa-adhB/P18pdc* produced 126 mM ethanol with the coproduction of PduABJknt, which compares to 85.23 mM ethanol produced without induction of the *pduABJknt* operon. It may be that the enhanced ethanol yield is a positive effect of tagged enzymes and BMC coproduction as the ethanogenic control strain MB001(DE3) containing untagged enzyme variants AdhB/Pdc showed slightly lower ethanol titers (104 mM). However, the production of PduABJknt in MB001(DE3)::P_{T7}*pduABJknt D18-GGSG-adhB/P18pdc*, a strain with a lower AdhB activity (Table 1), did not show enhanced ethanol production (85 mM ethanol in comparison to 89 mM ethanol without *pduABJknt* induction).

The ethanol production data represent preliminary work and the influence of different factors besides BMC production requires further investigation. For example, PduABJknt production had a moderate effect on growth under aerobic conditions (Fig. S7). The reduced growth due to BMC production might negatively influence final ethanol titers as observed for the control MB001(DE3)::P_{T7}*pduABJknt* P_{tuf}*adhB/pdc*. This strain produced 115.6 mM ethanol without PduABJknt coproduction and declined to 95.3 mM ethanol with PduABJknt coproduction. In *E. coli,* only a minor effect on growth was observed and ethanol production was successfully enhanced by BMC coproduction with P18Pdc/D18Adh (*12*). Another influence, which has to be further investigated are the P18 and D18 peptides itself, as they have been shown to form inclusion bodies when tagged to several enzymes (*21*).

Even though the ethanol titers observed in this study are far below previously obtained titers in *C. glutamicum* (*39*), this approach remains to be an interesting proof of principle of the application of Pdus for the optimization o heterologous pathways.

4 Conclusion

Redesigning and engineering BMCs for use in industrially relevant production strains like *C. glutamicum* has significant potential for extending the metabolic potential of the host, especially for pathways involving toxic or volatile intermediates. The propanediol utilization compartments have been extensively studied in their native host, *S. enterica*, whilst proof-of-principle approaches for heterologous gene transfer of the metabolosome operon of proteobacterial origin into the γ-Proteobacterium *E. coli* have been undertaken (*13, 15, 16, 28*). Very recently, we published the heterologous expression of a α-carboxysomal gene cluster from the Gram-negative γ-Proteobacterium *Halothiobacillus neapolitanus* in the Gram-positive Actinobacterium *C. glutamicum* (*40*) and now we have shown the successful transfer an operon between different phyla through alternating expression levels of *pduABJKNUT*. We observed that production the microcompartments in *C. glutamicum* even though their production can be optimized in order to prevent the co-occurrence of misshaped BMCs.

In this study we have contributed to the enhanced modularity of the system through the establishment of C-terminally localized synthetic interaction peptides as a targeting system and consequently shown that an increased variety of enzymes can be localised to BMCs without loss of function.

With their ability to form higher-order assemblies, PduA and $PduA_{lig}$*s* offer the possibility to be used as scaffolds onto which pathway enzymes can be targeted by C- or N-terminal targeting peptides, but their performance remains to be elucidated.

To contribute to advancements in metabolic engineering of pathways with toxic or volatile intermediates or pathways with competing reactions, BMCs have to be shown to be better than other microcompartment technologies (*21*) as well as encapsulation (*41*) and scaffolding strategies like common enzyme fusions (*29*), synthetic protein (*16, 42-44*) and DNA scaffolds (*45*).

5 Material and Methods

Bacterial strains, plasmids and growth conditions

All bacterial strains and plasmids used in this work are listed in Table S1. Synthetic compartments were established in the prophage free *C. glutamicum* MB001(DE3) strain containing a genomically integrated T7 polymerase (*46, 47*). Derivatives of this strain were constructed as indicated in Table S1. *C. glutamicum* was either cultivated in brain heart infusion (BHI, Difco Laboratories, Detroit, MI, USA) medium or CGXII medium (*48*) with 2% (w/v) glucose at 30 °C. For plasmid construction, *E. coli* DH5α was used. For all cloning procedures, the cells were cultivated in lysogeny broth (LB, (*49*)). If necessary, antibiotics were supplemented as followed: chloramphenicol (34 µg ml^{-1} for *E. coli*; 10 µg ml^{-1} for *C. glutamicum*), tetracycline (12.5 µg mL^{-1} for *E. coli*; 5 µg mL^{-1} for *C. glutamicum*), and kanamycin (50 µg mL^{-1} for *E. coli*; 25 µg mL^{-1} for *C. glutamicum*).

For cultivation of *C. glutamicum*, single colonies were obtained from agar plates after fresh transformation or streaked out from glycerol cultures. For preculture, 4 mL BHI medium were inoculated with a single colony and incubated for 8 hrs at 30 °C. Depending on purpose, the second preculture was prepared in 4 mL (for fluorescence microcopy, microtiter plate experiments, AdhB enzyme assays, TEM) or 20 mL (for compartment purifications) CGXII medium supplemented with 2% (w/v) glucose and inoculated to an OD_{600} of 1.

For growth experiments in the BioLector microbioreactor system (m2p labs, Baesweiler, Germany), 750 µL CGXII medium supplemented with 2% (w/v) glucose were inoculated with second preculture to a starting OD_{600} of 1 and cultivated in 48-well microtiter plates (Flower plates, m2p labs) at 30 °C and 1200 rpm for 24 h.

Recombinant DNA work and construction of chromosomal insertion strains

All routine methods such as PCR, DNA restriction and Gibson Assembly were performed according to manufacturer's instructions and standard protocols (*49, 50*). All primers used for plasmid construction are provided in the supplemental material together with construction details. Integrations into the *C. glutamicum* genome were performed with pK19*mobsacB* integration plasmids, which contained 500 bps of the integration sites flanking the sequences

484 of interest. The two homologous recombinations were performed as previously described (*51*).
485 The plasmids used in this work are listed in Table S1.

486 **AdhB and Pdc enzyme assay**

487 For AdhB and Pdc assays, cells of a 20 mL main culture (OD_{600} of 5) were harvested and snap-
488 frozen in liquid nitrogen until use. Subsequently, the cells were resuspended in 500 µL and
489 lysed using the bead mill homogenizer Precellys 24 (Peqlab, Bonn, Germany) at 6,000 rpm
490 three times for 20 seconds and cooled on ice in between. Cell lysate was collected by
491 transferring the supernatant to new Eppendorf tubes after centrifugation at 16.000 rpm for
492 30 min at 4 °C.
493 The AdhB assay was based on the work of Kinoshita *et al.* (*52*) but was performed in 96-well
494 microplate format and measured with the Infinite PRO 200 microplate reader (Tecan,
495 Männedorf, Switzerland). 20 µL of 1:20 diluted cell-free extract were mixed with 160 µL assay
496 buffer (50 mM Tris-HCl, pH 8.5, 10 mM NAD^+) and added to the plate. The reader was pre-
497 heated to 30 °C and the reaction was started with the addition of 20 µL 4% (v/v) ethanol
498 solution in 50 mM Tris-HCl, pH 8.5 via the injector system. The absorption at 340 nm was
499 measured directly after the addition of the substrate in 40 s intervals for 10 minutes. Technical
500 triplicates were used for each sample.
501 The Pdc assay (*53*) was conducted at 30 °C using the Infinite PRO 200 (Tecan, Männedorf,
502 Switzerland). 20 µL of diluted cell-free extract were mixed with 160 µL assay buffer (50 mM
503 potassium phosphate, pH 6.5, 0.15 mM NADH, 10 U/mL yeast ADH (Sigma Aldrich, St. Louis,
504 USA) solution). The reader was pre-heated to 30 °C and the reaction was started with the
505 addition of 20 µL 200 mM sodium pyruvate solution in assay buffer via the injector system. The
506 decrease in absorption at 340 nm was measured every 20 sec for 20 cycles. Technical
507 triplicates were used per sample.
508 For both assays, one unit of specific activity was defined as conversion of 1 µmol NAD^+ or
509 NADH per minute, respectively. Specific activity refers to the activity in the crude cell extract
510 per mg protein. Protein amount in the extracts were quantified with the Pierce™ BCA Protein
511 Assay Kit (Thermo Fisher Scientific, Waltham, USA) and BSA as protein standard.

Transmission electron microscopy

The main cultures (CGXII supplemented with 2% (w/v) glucose) were inoculated to an optical density at 600 nm of 1 and cultivated for 2 hrs at 30 °C. Compartment gene induction was triggered by the addition of 50 µM IPTG to the culture and the cells were cultivated for further 4 hrs. Bacteria were embedded, sectioned and stained as described previously (*12, 13*) with the addition of the application of a vacuum during the glutaraldehyde, osmium tetroxide and 100% resin steps. During these steps the pellets were resuspended in the appropriate solution and placed in a vacuum desiccator. A vacuum was applied for 1 min and released to aid infiltration of the solutions into the cells. This process was repeated twice before incubations in the aforementioned solutions and was carried out according to the protocol. Images were obtained using a JEOL-1230 transmission electron microscope equipped with a Gatan multiscan digital camera operated at an accelerating voltage of 80 kV.

Fluorescence microscopy

Main cultures for fluorescence microscopy analyses were performed in 20 mL CGXII supplemented with 2% (w/v) glucose inoculated to a starting OD_{600} of 1 in baffled shake flasks at 30 °C for 2 hrs. The production of shell and fluorescence proteins was induced with 50 µM IPTG and 50 ng ml^{-1} anhydrotetracycline for 4 hrs. To reduce the movement of the cells for microscopy, agar pads with 1% (w/v) agarose were prepared between two microscopy slides. 3 µL of a sample were placed on the agar pad and a cover slip was immediately placed above. The fluorescence microscopy has been performed with the AxioImager M2 microscope with AxioCam MRm using a Plan-Apochromat 100x, 1.40 Oil phase contrast oil-immersion objective (Carl Zeiss MicroImaging GmbH, Göttingen, Germany). The optimal exposure time for the different fluorescence images was determined with the automatic measurement option of the AxioVision Rel. 4.8 software (Carl Zeiss MicroImaging GmbH) and the pictures were analyzed with the same software.

Author Information

Corresponding Author

*Tel: +49 2461 615430. E-mail: j.frunzke@fz-juelich.de

Author contribution

I.H. and J.F. designed the experiments. I.H., D.J.P., K.N.L., and I.B. performed the experiments. I.H., J.F. and M.J.W. wrote the manuscript.

Notes

The authors declare no competing financial interest.

Acknowledgements

We acknowledge the financial support by the Helmholtz Association (grant VH-NG-716).

Supporting Information

Sequence S1: Synthesized ‘Protein_scaffolds$_{opt}$’ sequences; List of DNA sequences used for construction of respective plasmids;

Table S1: List of strains and plasmid used within this work, Relevant characteristics and source or reference;

Table S2: Number of cells with ‚BMC-like‘ structures; TEM images of different strains evaluated on occurrence of closed BMC-like structures within the cells;

Table S3: Amino acid distribution of different C- and N-terminal targeting peptides; Comparison of C17$_{K.p.}$, C17$_{P.m.}$, P18 and D18 peptides;

Tables S1-S6: Construction of used plasmids; Given are assembly procedure, primer pairs used for PCR and plasmid backbones;

Table S7: List of oligonucleotides used in this study;

Figure S1: Transmission electron microscopy of *C. glutamicum* MB001(DE3) showing a volutin granule and an unknown artefact;

Figure S2: Growth curves of different *C. glutamicum* MB001(DE3) Pdu production strains. Pdu production was induced with 50 µM IPTG.

Figure S3: PduABJknt purification approach; SDS-PAGE loaded with four protein fractions obtained during purification;

Figure S4: Fluorescence microscopy analysis of different *C. glutamicum* MB001(DE3)::P_{T7}*pduABJknt* strains*;* Different fluorescence reporter plasmids used;

Figure S5: TEM images of *C. glutamicum* MB001(DE3*)* *pduA*$_{lig}$*BJknt* strains with irregularly shaped BMCs;

Figure S6: Activity measurements of seven AdhB versions in crude cell extracts; AdhB was tagged with no, C-, or N-terminal targeting peptides;

Figure S7: Growth curves of several ethanol production and control strains; Aerobic cultivation; Induction of BMC production with 50 µM IPTG;

References

1. Cai, F., Sutter, M., Bernstein, S. L., Kinney, J. N., and Kerfeld, C. A. (2015) Engineering bacterial microcompartment shells: chimeric shell proteins and chimeric carboxysome shells, *ACS Synth. Biol. 4*, 444-453.
2. Kerfeld, C. A., and Erbilgin, O. (2015) Bacterial microcompartments and the modular construction of microbial metabolism, *Trends Microbiol. 23*, 22-34.
3. Kerfeld, C. A., and Melnicki, M. R. (2016) Assembly, function and evolution of cyanobacterial carboxysomes, *Curr. Opin. Plant Biol. 31*, 66-75.
4. Jorda, J., Lopez, D., Wheatley, N. M., and Yeates, T. O. (2013) Using comparative genomics to uncover new kinds of protein-based metabolic organelles in bacteria, *Protein Sci 22*, 179-195.
5. Havemann, G. D., Sampson, E. M., and Bobik, T. A. (2002) PduA is a shell protein of polyhedral organelles involved in coenzyme B(12)-dependent degradation of 1,2-propanediol in Salmonella enterica serovar typhimurium LT2, *J. Bacteriol. 184*, 1253-1261.
6. Frank, S., Lawrence, A. D., Prentice, M. B., and Warren, M. J. (2013) Bacterial microcompartments moving into a synthetic biological world, *J. Biotechnol. 163*, 273-279.
7. Crowley, C. S., Cascio, D., Sawaya, M. R., Kopstein, J. S., Bobik, T. A., and Yeates, T. O. (2010) Structural insight into the mechanisms of transport across the *Salmonella enterica* Pdu microcompartment shell, *J. Biol. Chem. 285*, 37838-37846.
8. Thompson, M. C., Cascio, D., Leibly, D. J., and Yeates, T. O. (2015) An allosteric model for control of pore opening by substrate binding in the EutL microcompartment shell protein, *Protein Sci. 24*, 956-975.
9. Tanaka, S., Sawaya, M. R., and Yeates, T. O. (2010) Structure and mechanisms of a protein-based organelle in *Escherichia coli*, *Science 327*, 81-84.
10. Havemann, G. D., Sampson, E. M., and Bobik, T. A. (2002) PduA is a shell protein of polyhedral organelles involved in coenzyme B-12-dependent degradation of 1,2-propanediol in *Salmonella enterica* serovar typhimurium LT2, *J. Bacteriol. 184*, 1253-1261.
11. Parsons, J. B., Dinesh, S. D., Deery, E., Leech, H. K., Brindley, A. A., Heldt, D., Frank, S., Smales, C. M., Lunsdorf, H., Rambach, A., Gass, M. H., Bleloch, A., McClean, K. J., Munro, A. W., Rigby, S. E., Warren, M. J., and Prentice, M. B. (2008) Biochemical and structural insights into bacterial organelle form and biogenesis, *J. Biol. Chem. 283*, 14366-14375.

12. Lawrence, A. D., Frank, S., Newnham, S., Lee, M. J., Brown, I. R., Xue, W. F., Rowe, M. L., Mulvihill, D. P., Prentice, M. B., Howard, M. J., and Warren, M. J. (2014) Solution structure of a bacterial microcompartment targeting peptide and its application in the construction of an ethanol bioreactor, *ACS Synth. Biol. 3*, 454-465.
13. Parsons, J. B., Frank, S., Bhella, D., Liang, M., Prentice, M. B., Mulvihill, D. P., and Warren, M. J. (2010) Synthesis of empty bacterial microcompartments, directed organelle protein incorporation, and evidence of filament-associated organelle movement, *Mol. Cell 38*, 305-315.
14. Held, M., Kolb, A., Perdue, S., Hsu, S. Y., Bloch, S. E., Quin, M. B., and Schmidt-Dannert, C. (2016) Engineering formation of multiple recombinant Eut protein nanocompartments in *E. coli*, *Sci. Rep. 6*, 24359.
15. Choudhary, S., Quin, M. B., Sanders, M. A., Johnson, E. T., and Schmidt-Dannert, C. (2012) Engineered protein nano-compartments for targeted enzyme localization, *PLoS One 7*, e33342.
16. Lassila, J. K., Bernstein, S. L., Kinney, J. N., Axen, S. D., and Kerfeld, C. A. (2014) Assembly of robust bacterial microcompartment shells using building blocks from an organelle of unknown function, *J. Mol. Biol. 426*, 2217-2228.
17. Fan, C., Cheng, S., Liu, Y., Escobar, C. M., Crowley, C. S., Jefferson, R. E., Yeates, T. O., and Bobik, T. A. (2010) Short N-terminal sequences package proteins into bacterial microcompartments, *PNAS 107*, 7509-7514.
18. Kinney, J. N., Salmeen, A., Cai, F., and Kerfeld, C. A. (2012) Elucidating essential role of conserved carboxysomal protein CcmN reveals common feature of bacterial microcompartment assembly, *J. Biol. Chem. 287*, 17729-17736.
19. Aussignargues, C., Paasch, B. C., Gonzalez-Esquer, R., Erbilgin, O., and Kerfeld, C. A. (2015) Bacterial microcompartment assembly: The key role of encapsulation peptides, *Commun. Integr. Biol. 8*, e1039755.
20. Fan, C., Cheng, S., Sinha, S., and Bobik, T. A. (2012) Interactions between the termini of lumen enzymes and shell proteins mediate enzyme encapsulation into bacterial microcompartments, *PNAS 109*, 14995-15000.
21. Lee, M. J., Brown, I. R., Juodeikis, R., Frank, S., and Warren, M. J. (2016) Employing bacterial microcompartment technology to engineer a shell-free enzyme-aggregate for enhanced 1,2-propanediol production in *Escherichia coli*, *Metab. Eng. 36*, 48-56.
22. Liang, M., Frank, S., Lunsdorf, H., Warren, M. J., and Prentice, M. B. (2017) Bacterial microcompartment-directed polyphosphate kinase promotes stable polyphosphate accumulation in *E. coli*, *Biotechnol. J. 12*, 10.
23. Yung, M. C., Bourguet, F. A., Carpenter, T. S., and Coleman, M. A. (2017) Re-directing bacterial microcompartment systems to enhance recombinant expression of lysis protein E from bacteriophage ϕX174 in *Escherichia coli*, *Microb. Cell Fact. 16*, 71.
24. Lee, J. Y., Na, Y. A., Kim, E., Lee, H. S., and Kim, P. (2016) The Actinobacterium *Corynebacterium glutamicum*, an Industrial Workhorse, *J. Microbiol. Biotechnol. 26*, 807-822.
25. Becker, J., and Wittmann, C. (2015) Advanced biotechnology: metabolically engineered cells for the bio-based production of chemicals and fuels, materials, and health-care products, *Angew. Chem., Int. Ed. Engl. 54*, 3328-3350.
26. Pang, A., Frank, S., Brown, I., Warren, M. J., and Pickersgill, R. W. (2014) Structural insights into higher order assembly and function of the bacterial microcompartment protein PduA, *J. Biol. Chem. 289*, 22377-22384.
27. Pallerla, S. R., Knebel, S., Polen, T., Klauth, P., Hollender, J., Wendisch, V. F., and Schoberth, S. M. (2005) Formation of volutin granules in *Corynebacterium glutamicum*, *FEMS Microbiol. Lett. 243*, 133-140.
28. Havemann, G. D., and Bobik, T. A. (2003) Protein content of polyhedral organelles involved in coenzyme B12-dependent degradation of 1,2-propanediol in *Salmonella enterica* serovar Typhimurium LT2, *J. Bacteriol. 185*, 5086-5095.
29. Otten, A., Brocker, M., and Bott, M. (2015) Metabolic engineering of *Corynebacterium glutamicum* for the production of itaconate, *Metab. Eng. 30*, 156-165.

30. Cheng, S., Sinha, S., Fan, C., Liu, Y., and Bobik, T. A. (2011) Genetic analysis of the protein shell of the microcompartments involved in coenzyme B12-dependent 1,2-propanediol degradation by *Salmonella*, *J. Bacteriol. 193*, 1385-1392.
31. Kim, E. Y., Jakobson, C. M., and Tullman-Ercek, D. (2014) Engineering transcriptional regulation to control Pdu microcompartment formation, *PLoS One 9*, e113814.
32. Hentschel, E., Will, C., Mustafi, N., Burkovski, A., Rehm, N., and Frunzke, J. (2013) Destabilized eYFP variants for dynamic gene expression studies in *Corynebacterium glutamicum*, *Microb Biotechnol 6*, 196-201.
33. Herman, C., Thevenet, D., Bouloc, P., Walker, G. C., and D'Ari, R. (1998) Degradation of carboxy-terminal-tagged cytoplasmic proteins by the *Escherichia co*li protease HflB (FtsH), *Genes Dev. 12*, 1348-1355.
34. Dueber, J. E., Wu, G. C., Malmirchegini, G. R., Moon, T. S., Petzold, C. J., Ullal, A. V., Prather, K. L., and Keasling, J. D. (2009) Synthetic protein scaffolds provide modular control over metabolic flux, *Nat. Biotechnol. 27*, 753-759.
35. Orita, I., Sakamoto, N., Kato, N., Yurimoto, H., and Sakai, Y. (2007) Bifunctional enzyme fusion of 3-hexulose-6-phosphate synthase and 6-phospho-3-hexuloisomerase, *Appl. Microbiol. Biotechnol. 76*, 439-445.
36. James, C. L., and Viola, R. E. (2002) Production and characterization of bifunctional enzymes. Substrate channeling in the aspartate pathway, *Biochemistry 41*, 3726-3731.
37. Chen, A. H., and Silver, P. A. (2012) Designing biological compartmentalization, *Trends Cell Biol. 22*, 662-670.
38. Lee, H., DeLoache, W. C., and Dueber, J. E. (2012) Spatial organization of enzymes for metabolic engineering, *Metab. Eng. 14*, 242-251.
39. Inui, M., Kawaguchi, H., Murakami, S., Vertes, A. A., and Yukawa, H. (2004) Metabolic engineering of *Corynebacterium glutamicum* for fuel ethanol production under oxygen-deprivation conditions, *J. Mol. Microbiol. Biotechnol. 8*, 243-254.
40. Baumgart, M., Huber, I., Abdollahzadeh, I., Gensch, T., and Frunzke, J. (2017) Heterologous expression of the *Halothiobacillus neapolitanus* carboxysomal gene cluster in *Corynebacterium glutamicum*, *J. Biotechnol. 27*, 30124-30124.
41. Wang, Y., Heermann, R., and Jung, K. (2017) CipA and CipB as scaffolds to organize proteins into crystalline inclusions, *ACS Synth. Biol.*
42. Moon, T. S., Dueber, J. E., Shiue, E., and Prather, K. L. (2010) Use of modular, synthetic scaffolds for improved production of glucaric acid in engineered *E. coli*, *Metab. Eng. 12*, 298-305.
43. Price, J. V., Chen, L., Whitaker, W. B., Papoutsakis, E., and Chen, W. (2016) Scaffoldless engineered enzyme assembly for enhanced methanol utilization, *PNAS 113*, 12691-12696.
44. Yang, Z., Gao, X., Xie, H., Wang, F., Ren, Y., and Wei, D. (2017) Enhanced itaconic acid production by self-assembly of two biosynthetic enzymes in *Escherichia coli*, *Biotechnol. Bioeng. 114*, 457-462.
45. Conrado, R. J., Wu, G. C., Boock, J. T., Xu, H., Chen, S. Y., Lebar, T., Turnsek, J., Tomsic, N., Avbelj, M., Gaber, R., Koprivnjak, T., Mori, J., Glavnik, V., Vovk, I., Bencina, M., Hodnik, V., Anderluh, G., Dueber, J. E., Jerala, R., and DeLisa, M. P. (2012) DNA-guided assembly of biosynthetic pathways promotes improved catalytic efficiency, *Nucl. Acids Res. 40*, 1879-1889.
46. Kortmann, M., Kuhl, V., Klaffl, S., and Bott, M. (2015) A chromosomally encoded T7 RNA polymerase-dependent gene expression system for *Corynebacterium glutamicum*: construction and comparative evaluation at the single-cell level, *Microb Biotechnol 8*, 253-265.
47. Baumgart, M., Unthan, S., Ruckert, C., Sivalingam, J., Grunberger, A., Kalinowski, J., Bott, M., Noack, S., and Frunzke, J. (2013) Construction of a prophage-free variant of *Corynebacterium glutamicum* ATCC 13032 for use as a platform strain for basic research and industrial biotechnology, *Appl. Environ. Microbiol. 79*, 6006-6015.
48. Keilhauer, C., Eggeling, L., and Sahm, H. (1993) Isoleucine synthesis in *Corynebacterium glutamicum* - Molecular analysis of the *IlvB-IlvN-IlvC* operon, *J. Bacteriol. 175*, 5595-5603.

49. Sambrook, J., and Russell, D. W. (2001) *Molecular cloning: A laboratory manual*, 3rd ed., Cold Spring Harbor Laboratory Press, NY.
50. Gibson, D. G., Young, L., Chuang, R. Y., Venter, J. C., Hutchison, C. A., 3rd, and Smith, H. O. (2009) Enzymatic assembly of DNA molecules up to several hundred kilobases, *Nat. Methods 6*, 343-345.
51. Niebisch, A., and Bott, M. (2001) Molecular analysis of the cytochrome bc1-aa3 branch of the *Corynebacterium glutamicum* respiratory chain containing an unusual diheme cytochrome c1, *Arch. Microbiol. 175*, 282-294.
52. Kinoshita, S., Kakizono, T., Kadota, K., Das, K., and Taguchi, H. (1985) Purification of two alcohol dehydrogenases from *Zymomonas mobilis* and their properties, *Appl. Microbiol. Biotechnol. 22*, 249-254.
53. Talarico, L. A., Gil, M. A., Yomano, L. P., Ingram, L. O., and Maupin-Furlow, J. A. (2005) Construction and expression of an ethanol production operon in Gram-positive bacteria, *Microbiology 151*, 4023-4031.

Tables

Table 1: Specific activity of AdhB and Pdc versions in cell-free extracts of MB001(DE3). Presented are mean values and standard deviations of triplicate measurements with cell extracts of three independent cultures.

AdhB production plasmid	Specific activity U mg protein^{-1}	Pdc production plasmid	Specific activity U mg protein^{-1}
pVWEx2-P$_{tuf}$-*adhB*	0.376 ± 0.045	pVWEx2-P$_{tuf}$-*pdc*	0.549 ± 0.042
pVWEx2-P$_{tuf}$-*D18-GSGS-adhB*	0.041 ± 0.009	pVWEx2-P$_{tuf}$-*P18-NdeI-pdc*	0.696 ± 0.046
pVWEx2-P$_{tuf}$-*D18-10AS-adhB*	0.067 ± 0.005	pVWEx2-P$_{tuf}$-*P18-GS-pdc*	0.541 ± 0.104
pVWEx2-P$_{tuf}$-*D60-adhB*	0.021 ± 0.009	pVWEx2-P$_{tuf}$-*P18-GSGS-pdc*	0.518 ± 0.082

Figure legends

Figure 1: A Different Pdu operon designs. The whole Pdu operon consists of 21 genes, encoding different shell proteins (yellow), enzymes for 1,2-propanediol degradation (blue) and proteins with other functions (grey). The seven shell proteins were described to self-assemble to hexameric compartment structures also in the absence of cargo proteins. The whole operon and the different *pdu* shell operon versions were expressed in *C. glutamicum*. **B** Coproduction of P18eYFP with different Pdu operons in MB001(DE3) background. The protein production was induced after 2 hrs of cultivation in CGXII + 2% (w/v) glucose with 50 µM IPTG and 50 ng mL^{-1} anhydrotetracycline and strains were cultivated for 4 hrs after induction. Scale bar is 2 µm. *pduA-X*: native 21 gene operon*; pduABJKNUT:* synthetic operon contains 40 bp upstream regions including a RBS in front of *pduAB*, p*duJ*, *pduK*, *pduN*, *pduU* and *pduT*; $pduABJKNTU_{native}$: synthetic shell operon with native 3' untranslated regions (3'UTR) of the shell genes.

Figure 2: Transmission electron microscopy analysis of MB001(DE3) WT (a) and different MB001(DE3) Pdu production strains (b-j). The cells were grown in CGXII with 2% glucose for 4 hrs after induction of Pdu production with 50 µM IPTG. Downregulation of different genes are indicated by lower cases. (a) MB001(DE3) WT; (b) *pduABJKNUT*; (c) *pduABJKnut;* (d) *pduABJKnt*; (e) *pduABJkNut*; (f) *pduABJkNu*; (g) *pduABJknt*; (h) *pduABJkNt*; (i) *pduABJkn*; (j) *pduABJkN*.

Figure 3: Characterization of BMC production strain MB001(DE3)::P_{T7}*pduABJknt.* (a) Growth of MB001(DE3) (grey) MB001(DE3)::P_{T7}*pduABJknt* (green) and MB001(DE3)::P_{T7}*pduA* (red) induced with 0, 20, 50 or 150 µM IPTG. The optimized Pdu operon variant and the *pduA* gene were chromosomally integrated into the intergenic region between cg1121 and cg1122. (b) Fluorescence microscopy analysis to determine the distribution of D18eYFP/P18eYFP variants with coproduction of PduABJknt (50 µM IPTG). Scale bar is 2 µm. ASV: SsrA-degradation tag variant AAEKSQRDYAASV; (c) Thin sections of MB001(DE3)::P_{T7}*pduABJknt*. Cells were grown in CGXII 2% glucose for 4 hrs after induction of Pdu production with 50 µM IPTG.

Figure 4: Fluorescence microscopy analysis of PduABJknt production strains. The fluorescence reporter eYFP was used to determine the localization of eYFP fused with different C- and N-terminal targeting peptides during coproduction of PduABJknt (50 µM IPTG) in MB001(DE3). P18eYFP, eYFP-P18 and eYFP-$C17_{K.p.}$ showed localization in the mid part of the cell.

Figure 5: Production of $PduA_{lig}$-BJknt BMCs and establishment of C-terminal targeting strategies. Thin sections of (a) MB001(DE3) $pduA_{PDZlig}$*BJknt* (b) MB001(DE3) $pduA_{GBDlig}$*BJknt* and (c) MB001(DE3) $pduA_{SH3lig}$*BJknt* reveal BMC-like structures within the cytosol 4 hrs after induction of protein production with 50 µM IPTG. (d) Localization of C- and N-terminally targeted eYFP (D18eYFP, P18CFP, $eYFP_{dom}$) to the cognate $PduA_{lig}$-BJknt BMCs. The fluorescence pattern was similar to those of the control MB001(DE3) *pduABJknt D18eyfp-P18cfp*.

Figure 6: PduA and PduJ form filaments in *C. glutamicum*. (a) Upon induction with 50 µM IPTG, MB001(DE3) *pduA* produced large bundles of regular filaments. (b) PduJ formed a mixture of linear filaments and rolled protein sheets. P18eYFP and D18eYFP colocalize to filamentous PduA structures (c) but not to (d) PduJ filaments. Scale bar for fluorescence microscopy images is 2 µm.

Figure 7: Distribution of eYFP$_{dom}$ with coproduction of the cognate PduA$_{lig}$ version. eYFP$_{PDZdom}$ and eYFP$_{GBDdom}$ localize to the respective PduA$_{lig}$ filaments. PduA$_{SH3lig}$ seemed not to form filaments, as neither eYFP$_{SH3dom}$ nor D18eYFP showed a distinct localization within the cytosol. Scale bar is 2 µm.

Figure 8: Application of optimized Pdu compartments for ethanol production in *C. glutamicum*. Strains MB001(DE3) and MB001(DE3)::P$_{T7}$*PduABJknt* were compared and tested with the enzyme combinations Pdc/AdhB, D18-10aa-AdhB/P18Pdc and D18-GGSG-AdhB/Pdc. Ethanol production was assayed under 'semi-anaerobic' conditions with and without coproduction of BMCs. Dark grey: 50 µM IPTG; light grey: 0 µM IPTG; ethanol content was measured for two biological replicates for each strain and condition. Error bars represent the range of the two measured samples.